RAPID SODIUM CHANNEL CONDUCTANCE CHANGES DURING VOLTAGE CLAMP STEPS IN SQUID GIANT AXONS

JURGEN F. FOHLMEISTER AND WILLIAM J. ADELMAN, JR.
Laboratory of Biophysics, National Institutes of Health at the Marine Biological Laboratory, Woods Hole, Massachusetts 02543 and Laboratory of Neurophysiology, University of Minnesota, Minneapolis, Minnesota 55455

ABSTRACT The sodium conductance of the membrane of the giant axon of squid was isolated by the use of potassium-free solutions and voltage-clamped with pulses containing three levels of depolarization. The conductance appears to undergo rapid changes during certain repolarizing clamp steps whose voltage reach at least partially overlaps the gating range. The percentage change in conductance increases with time of depolarization from ~0 to ~25–30% at 7 ms for a potential step from +70 to −30 mV. Conductance steps were also observed for voltage steps from various depolarized levels to −70 mV. All observed shifts were in the direction of a decreased conductance. The conductance steps appear to be a weak function of the concentration of external calcium, which also acts as a voltage-dependent channel blocker for inwardly directed sodium currents. A number of possible mechanisms are suggested. One of these is discussed in some detail and postulates a voltage- and time-dependent molecular process that does not itself yield open or closed channel conformations, but that affects the magnitude of the rate constants that do connect open and closed state conformations.

INTRODUCTION

Voltage-clamp of excitable membranes has been primarily concerned with the measurement of the relaxation of conductance changes following steps in membrane potential (Hodgkin and Huxley, 1952). Because these conductance changes are observed to occur on a time scale of milliseconds (plus or minus an order of magnitude), it has been generally assumed that the conductance varies by only a negligible amount during the time necessary to generate the command voltage change on the scale of 1 μs. We report here the observation that the sodium conductance of the squid axon membrane appears to undergo a "step" change during certain voltage-steps that are commanded after a period of depolarization. The rapid conductance change itself is similar to the conductance change that occurs in the presence of certain blocking ions (e.g., Ca^{++} for the sodium channel, Taylor et al., 1976, or Cs^{+} for the potassium channel, Adelman and French, 1978) when the voltage is changed. However, its strong dependence on the voltage history is characteristically distinct from the action of blocking ions. The finding appears to imply that the membrane model, consisting of a single population of Na channels with a single conducting state and with no delayed potential energy adjustments to either gating or ion-flux barriers within the membrane, is inadequate. Ways in which these conditions may be relaxed are presented in the discussion.

Correspondence should be sent to Dr. Fohlmeister, Department of Physiology, University of Minnesota, Minneapolis, MN 55455.

METHODS

Cleaned, single giant axons from the hindmost stellar nerve of the squid *loligo pealei* were perfused and superfused with K-free solutions and voltage-clamped using pulses with three voltage levels, as shown in Fig. 1. All depolarizing pulses were followed by two hyperpolarizing pulses with the same form (apart from the overall minus sign) but of exactly half amplitude of the depolarizing pulse. The half amplitude limited all hyperpolarizations to membrane potentials greater than or equal to −140 mV. Algebraic summation of the currents from the group of three pulses eliminated all linear current components including leakage and capacitative transients. All pulses were spaced by 3 s.

Series resistance, R_s, was compensated for as a voltage by means of a feedback amplifier that monitored the membrane current at the output of the current-to-voltage transducer through an impedance converter, so as not to degrade the membrane current measurement. This system was calibrated to fully compensate for the series resistances in an RC model membrane circuit. The model circuit has a variable series resistance adjustable to a set of known values. The criterion used for calibration was that the voltage across the model membrane capacitance remained constant, irrespective of the value of the parallel membrane resistance (adjustable to passive or active equivalent states). A frequently run test of the system involved setting the model R_s to some unknown value and then adjusting the clamp for 100% compensation. In such cases, the value of the unknown could be determined to ~1% accuracy.

A nomograph of squid axon R_s values determined as a function of membrane area (axon diameter) and various external and internal ionic strength solutions was used to adjust the voltage clamp R_s compensation. Experimental determination and justification for the use of these R_s

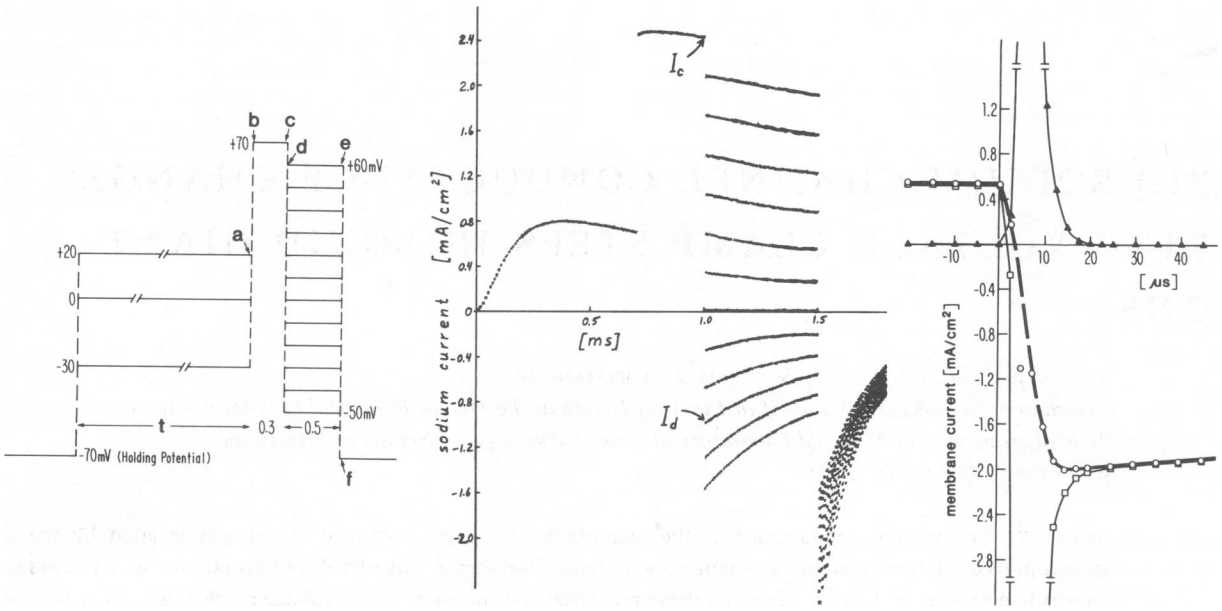

FIGURE 1 *Left*: voltage-clamp pulse profiles (only depolarizing pulses are shown). *Center*: current records for a clamp series of V_3 of the pulse profile. Groups of three pulses (one depolarizing and two half-amplitude hyperpolarizing, see text) were algebraically summed for these records. Conditioning depolarization, V_1, is +20 mV, $[Na]_i = [Na]_e = 450$ mM, $[Ca]_e = 10$ mM and $t = 0.7$ ms. Currents I_c and I_d indicate the points of measurement for the ratios, I_c/I_d, defined in the results. *Right*: current transitions across step $c \rightarrow d$ of the pulse profile with $E(c) = +70$ and $E(d) = -30$ mV. □, ▲: membrane currents for depolarizing and half-amplitude hyperpolarizing voltage pulses, respectively. ○: algebraically summed current from three (one depolarizing and two half-amplitude hyperpolarizing) pulses. $[Na]_e = 450$ mM, $[Na]_i = 50$ mM, $[Ca]_e = 4$ mM, and $t = 0.7$ ms.

values is given in Binstock et al. (1975). The values given in Binstock et al. were shown by Adelman et al. (1977) to have a basis in the anatomy of the Schwann cell layer and external connective tissue. Extension of these values to solutions with other ionic strengths is given in Fohlmeister and Adelman (1982 *a*).

The use of the RC model circuit also indicated that our voltage clamp system showed oscillations or instability only when the R_s compensation exceeded the actual model R_s value. This was true over a selected range of R_s values from 0 to 10 Ω cm². Our criterion of real axon clamp stability was that the membrane current transient settled within 10 μs for hyperpolarized voltage steps and that the sodium current was smooth and continuous at all values of step depolarizations with no sodium-current thresholds, delays, bumps, or higher-order oscillations. As the current was measured with an external plate electrode only 1 mm in length between two 5-mm grounded guard electrodes, and as the internal voltage electrode (V_{int}) was completely separated from the axial wire electrode, common errors due to axial-wire-to-V_{int}-electrode cross-talk and long external current electrode averaging were avoided. This overall system has been described by Adelman and French (1978). The external plate electrodes were fabricated on the basis of Fig. 3:81 and Eq. 3:11 in Cole (1968) and plated according to the method described by Cole and Kishimoto (1962). The V_{int} and the external voltage measuring electrodes were fabricated by the method of Fishman (1973).

The following series resistances were compensated for where the solution ratios refer to millimolar external Na/millimolar internal Na: 1.6 Ω cm² for 450/450 solutions, 2.0 Ω cm² for 450/150 and 100/150 solutions, and 2.4 Ω cm² for 450/50 and 100/50 solutions (see Table I and Fig. 3). Temperature was maintained within ±0.05°C of a calibrated value of 5°C.

Data were acquired for eight different external solutions. These consisted of two calcium series (100, 40, 10, and 4 mM Ca^{++} with 450 mM and 100 mM Na^+ (Table I). All were K^+ free and Mg^{++} free, and one of them was Cs^+ free.

Three different internal solutions that may be distinguished by their Na^+ concentrations (450, 150, and 50 mM) were used. The solutions were K^+ free with Cs^+ used as a replacement for potassium. The 450 mM Na^+ internal solution was Cs^+ free. The composition of perfusing solutions is also given in Table I.

In addition to the data presented in the results, experiments were performed with combinations of solutions $[Na]_e/[Na]_i = 100/150$ and

TABLE I
EXTERNAL SOLUTIONS (pH = 7.0)

Na^+	Ca^{++}	Cs^+	Cl^-	Tris	OsM
450	4	73	531	10	879
·	10	65	535	·	880
·	40	20	550	·	896
·	100	0	650	·	996
100	4	423	531	10	844
·	10	415	535	·	853
·	40	370	550	·	845
·	100	280	580	·	845

INTERNAL SOLUTIONS (pH = 7.2)

Na^+	HPO_4^{--}	$Glut^-$	F^-	Cs^+	Sucrose	OsM
50	10	30	100	100	680	1,014
150	25	100	150	150	505	991
450	50	300	50	0	270	930

All values are in millimoles per liter.

100/50, all millimolar. The pattern of conductance changes (percent changes) observed with these solutions were identical to those given in the results, but the error bars were approximately doubled when compared with those of $[Na]_e/[Na]_i$ = 450/450 and 450/150, respectively. The reduced membrane current experiments were performed in part as a confirmation that the particular series resistance compensations used were not contributing to the observed effects.

The initial perfusion was carried out with a 300 mM K^+ plus 505 mM sucrose solution as perfusate and artificial sea water (ASW) externally (for example, see Fohlmeister and Adelman, 1982 *b*). The perfusate was then changed to one of the Kfree solutions (Table I) and the open-circuit membrane potential was observed to reach or cross 0 mV within 10 s. Upon reaching 0 mV the membrane was slowly (~2 s) clamped to a holding potential of −70 mV and held for ≥10 min before any data acquisition, to avoid any changes associated with Na-channel slow gating. The open-circuit resting potential was occasionally monitored during the course of an experiment followed each time by a 10-min holding period at −70 mV. Upon completion of data acquisition, the clamp circuit was opened, the axon reperfused with 300 mM K^+, and the resting potential was observed to return to the range of −55 to −65 mV in all cases. However, K-channel gating did not reappear.

The depolarizing pulses consisted of steps from a holding potential of −70 to −30 mV (for times t = 0, 0.4, 1.0, 2.5, 4.5, 7.0, 9.0, 12.0 ms), 0 or +20 mV (for t = 0.3, 0.7, 1.2, 2.0 3.0, 5.0, and 7.0 ms), followed by a step to +70 mV for 0.3 ms (Fig. 1). Instantaneous current-voltage (I-V) data were obtained immediately following the +70 mV potential by stepping to one of a series of potentials in the range of $-50 \leq E < +70$ mV for 0.5 ms before stepping back to the holding potential. These instantaneous I-V data served several purposes (see below and Results), among them to determine the shift in E_{Na} as a function of t due to periaxonal space Na accumulation or depletion and other unstirred layer effects. Shifts in sodium concentration in the periaxonal space were also calculated from the equation

$$[Na]_{space}(t) = [Na]_e + \frac{1}{\theta F}\int_{-\infty}^{t} I_{Na}(t') \cdot \exp\left[-(t - t')/\tau\right] dt' \quad (1)$$

where I_{Na} are measured values of sodium current (inwardly directed is negative), τ = 10 ms and θ = space width ≐ 200 Å (Fohlmeister and Adelman, 1982 *b*) as a consistency check on the interpretation that shifts in E_{Na} are indeed due to unstirred layer effects.

Because this paper deals with rapid conductance changes during a voltage step, the tuning of the clamp (response to step commands) was of primary importance. We attempted to achieve a critical damping of the current trace following the capacitative transient. With some axons we were dissatisfied with the relative slowness of the step under critical damping, and in those cases we allowed a small degree of oscillation with the voltage overshoot being <5% of the step value. In this way a settling time of ≤ 10 μs was obtained in all cases. Examples of current transients are shown in Fig. 1.

Current values at points *b*, *d*, and *f* (Fig. 1) were read 15 μs after the voltage step command. Although extrapolated values (across the 15 μs gap) were not used in data reduction, they are plotted as the dashed lines in Fig. 2. For certain voltage steps the difference between the extrapolated value and the 15 μs value was judged to be too large to allow a determination of the conductance shift across the step.

In the process of data reduction, sodium current is converted to conductance that, under special circumstances and certain assumptions, is interpreted as a probability that a randomly chosen single sodium channel is open. The conductance used is the chord conductance defined by

$$g_{Na}^{chord} \equiv I_{Na}/(E - E_{Na}). \quad (2)$$

The phenomenon presented in the results may have its origin in a number of possible mechanisms. Notable among these is the possibility of several distinct populations of Na channels with distinct instantaneous I-V characteristics (cf. Discussion). Nevertheless, until the existence of multiple populations is firmly established, it is incumbent upon us to describe the implications for the kinetics, assuming a single population of channels, each of which is either fully open or closed (Sigworth and Neher, 1980). We assume that a channel is nonconducting when the channel is gated closed and/or it is blocked by a blocking ion. For each channel molecule, both processes are assumed to be all-or-none, voltage dependent, and stochastic. The current, I_{Na}, is parametrized as

$$I_{Na} = \hat{g}_{Na} \cdot Q_{Na} \cdot (1 - r_{BL}) \cdot f_{Na} \quad (3)$$

where $\hat{g}_{Na}$ is a proportionality constant with the dimensions of conductance, Q_{Na} is the probability that a randomly chosen single Na channel is gated open ($0 \leq Q_{Na} \leq 1$), r_{BI} is the fraction of gated open channels that are blocked due to the presence of blocking ions and therefore nonconducting ($0 \leq r_{BI} \leq 1$), and f_{Na} is the voltage-dependent driving force with dimensions of voltage. From instantaneous current-voltage relations, which were measured under all experimental conditions reported herein (see Results, Fig. 5), we conclude that calcium acts as a blocking ion of the Na channel in such a way that $r_{BI} \to 0$ as $[Ca^{++}]_e \to 0$. Further, instantaneous current-voltage data obtained for t = 0 show that f_{Na} follows closely the form predicted by the constant field flux equation

$$f_{Na} = E\,\frac{[Na]_e/[Na]_i - \exp(eE/kT)}{1 - \exp(eE/kT)}. \quad (4)$$

We wish to draw no conclusions from this finding other than that this form of f_{Na} equals $E - E_{Na}$ only for symmetrical sodium concentrations ($[Na]_i = [Na]_e$) for which $E_{Na} = 0$. Therefore, combining Eqs. 2 and 3 under conditions of $r_{BI} = 0$, yields

$$g_{Na}^{chord} = \hat{g}_{Na} \cdot Q_{Na} \quad (5)$$

provided that $[Na]_i = [Na]_e$. The product $\hat{g}_{Na}Q_{Na}$ is used synonymously with chord conductance derived from currents recorded under these particular circumstances. Only when a single population of Na channels is assumed in the analysis does Q_{Na} take on its open-channel probability interpretation.

RESULTS

Current Transitions for *E* Step +70 → −30 mV

Fig. 2 gives plots of ionic currents measured at points *a*, *c*, and *d* of the voltage-clamp pulses as functions of t (*a*, *c*, *d*, and t are defined in Fig. 1). The curves *a* give the ordinary Na current associated with depolarizations of +20 and −30 mV as functions of t. Curves *c* and *d* decrease in magnitude towards zero current with increasing t. The classic interpretation of the decrease is that it is due to channel inactivation as a consequence of the depolarization for the time period t + 0.3 ms. In this interpretation the final 0.3 ms at +70 mV is assumed to "open" the Na-activation "gates" maximally with only a small effect on the slower inactivation "gates." (Current records do indeed suggest that the activation has approached a new steady state at the end of the 0.3 ms pulse.) The time course for the development of inactivation appears to have a small sigmoidal component (curves *c* and *d*, Fig. 2) that is somewhat more pronounced for the smaller conditioning

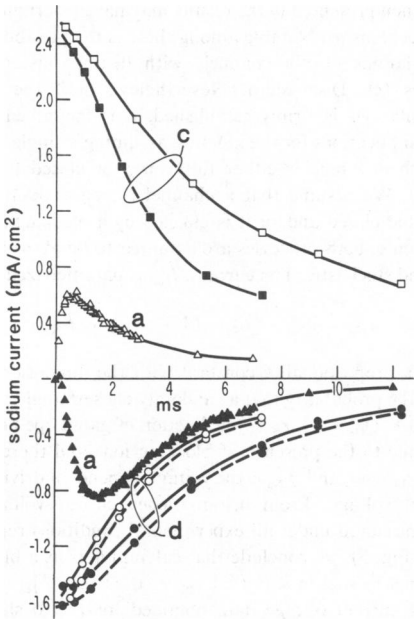

FIGURE 2 Sodium currents at points *a*, *c*, and *d* of the pulse profile (Fig. 1) as functions of the duration, *t*, of the conditioning depolarization. Curves *a* represent normal sodium currents following depolarizations to −30 mV (▲) and to +20 mV (△). Curves *c* are effectively "maximum" currents at the end of the 0.3 ms depolarization to +70 mV following a conditioning potential of −30 mV (□) and +20 mV (■). Curves *d* represent initial values of tail currents at −30 mV during the third level of depolarization. Conditioning potentials for curves *d* were −30 mV (●) and +20 mV (○). Currents for the solid lines (—) of curves *d* were taken at 15 μs following the voltage step command *c* → *d*. Dashed curves (---) represent extrapolations of the current traces to zero μs. $[Na]_i = [Na]_e$ = 450 mM and $[Ca]_e$ = 10 mM. A junction potential (subsequently measured to be 10 mV) was not compensated for this axon. All other experiments and data presented herein were compensated for the measured junction potentials. Current ratios, $[I_c/I_d](t)$, defined in the text, are quotients of values of a curve *c* and the corresponding curve *d* as functions of *t*.

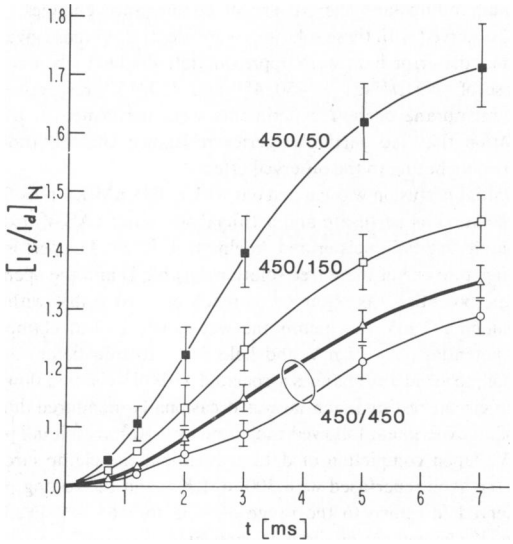

FIGURE 3 Normalized ratios of currents, $[I_c/I_d]_N$, measured at *c* and at *d* (see Fig. 1) as functions of *t*. Conditioning depolarizations (of *t* ms duration) were +20 mV (○, □, ■) and 0 mV (△). Membrane potentials at points *c* and *d* were +70 and −30 mV, respectively. The ratios defining the curves give $[Na]_e/[Na]_i$ in millimoles per liter. Each curve was separately normalized to 1.0 at *t* = 0. The data for the open triangles (△) were obtained under conditions of zero sodium current ($E = E_{Na}$) during the conditioning depolarization. When corrected for unstirred layer effects, the curves all coincide with the heavy curve defined by open triangles (△). The deviation of this curve from unity implies a *t*-dependent conductance step has occurred between points *c* and *d* spaced by 15 μs (see text). Error bars equal one standard deviation in the scatter among six axons for each curve.

depolarization of −30 mV. This time course may be related to the sigmoidal recovery from inactivation as previously described by Schauf (1974) and Chiu (1976).

Figs. 3 and 4 give plots of the ratios of currents, $[I_c/I_d]_N$, as functions of *t*, with $I_c(t)$ (the currents at point *c* [+70 mV]) and $I_d(t)$ (the currents at point *d* [−30 mV]) separated by 15 μs (Fig. 1). Individual curves, corresponding to different ionic environments, are each normalized to unity at *t* = 0 to compare percentage differences in their time development more easily. In all cases, the current ratios increase with increasing *t*. The different time developments among the current ratios in Fig. 3 can be explained on the basis of differential unstirred surface layer effects (see Instantaneous Current-Voltage Curves, below). When these effects are compensated for, the curves all coincide with the central curve, defined by open triangles. The behavior of this corrected curve implies that a conductance step occurs during the voltage step from +70 to −30 mV for all *t* with the possible exception of one (see Conductance Steps below). This follows because, if conductance remains constant between the measurements at points *c* and *d*, a flat (corrected) current ratio would necessarily result. Indeed, a nonflat curve will occur only if the percentage change in conductance varies with *t*.

The degree of the increase of $[I_c/I_d]_N$ with increasing *t*

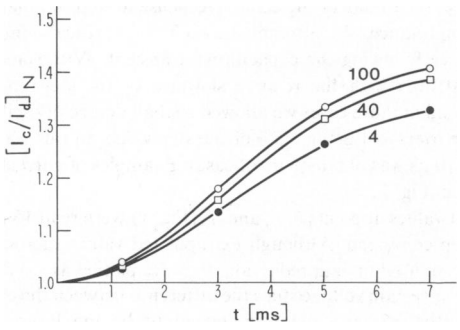

FIGURE 4 Current ratios, $[I_c/I_d]_N$, normalized to unity at *t* = 0 (see Fig. 3 and text) as functions of *t* for the three calcium concentrations of 100 (○), 40 (□) and 4 mM (●). Data were obtained with 450 mM sodium on both membrane sides with a conditioning depolarization of 0 mV. Thus membrane current was ~0 during the conditioning pulse, thereby obviating corrections due to unstirred layers (cf. Fig. 3). Membrane potentials at points *c* and *d* were +70 and −30 mV, respectively. Note the systematic increase of $[I_c/I_d]_N$ with increasing $[Ca]_e$ and *t* (see text).

appears also to be a function of the external Ca^{++} concentration as shown in Fig. 4. The differential effect between 4, 40, and 100 mM Ca^{++}, when combined with the corresponding curve for 10 mM Ca^{++} in Fig. 3, shows a systematic calcium-dependent shift with the larger effect for higher external calcium.

Instantaneous Current-Voltage Relations

Instantaneous I-V curves were measured immediately after point *c* (Fig. 1) with the following results:

(*a*) Instantaneous I-V curves are linear for symmetric Na concentrations ($[Na]_i = [Na]_e = 450$ mM) with $[Ca]_e = 4$ mM and for $t = 0$ and 1 ms (cf. Fig. 5). For larger t ($t = 7$ ms), the reversal potential is observed to shift somewhat, with the amount and direction depending on the potential of initial depolarization and the Na concentrations. Further, the curves are no longer linear throughout their entire range, even when there is no shift in E_{Na}.

The shift in E_{Na} can be accounted for on the basis of a sodium concentration shift across the membrane as a result of the sodium current during the initial depolarization. The concentration shift in the periaxonal space was computed numerically using Eq. 1 (Methods). The calculated shift for inwardly directed currents ($E = -30$ mV) amounts to a reduction from 450 to ~440 mM Na^+ in the periaxonal space at $t = 7$ ms. This amount is nearly independent of the internal sodium concentration, since the current magnitudes were roughly comparable for all $[Na]_i$. On the further assumption of a 10-mM increase at the internal membrane surface, the calculated shift in E_{Na} is about -1.07 mV for $[Na]_i = 450$ mM, -2.1 mV for 150 mM, and -4.9 mV for 50 mM. These estimates agree with the measured shifts of the reversal potentials. For smaller t (≤ 7 ms) the E_{Na} shift is correspondingly smaller. For outwardly directed currents ($[Na]_i = [Na]_e = 450$ mM and $E = +20$ mV) the E_{Na} shift is positive. The resulting change in driving force accounts for the differences among the curves of Fig. 3.

(*b*) The presence of relatively high external concentrations of calcium causes a partial blockade for inwardly directed sodium currents (cf. Taylor et al., 1976). The instantaneous I-V curves of Fig. 5 show this blocking action in the presence of 100 mM Ca^{++}. This pattern of calcium blockade is a systematic function of the calcium concentration and persists for all values of t.

(*c*) For unsymmetrical sodium concentrations the instantaneous I-V curves deviate from linearity in the direction predicted by the constant field flux equation (Methods, Eq. 4). Indeed, the experimental curves closely follow those predicted by the "constant field flux" equation for outwardly directed, and small inwardly directed driving forces, provided t is small. Deviations due to calcium block are observed for moderate to large inwardly directed driving forces.

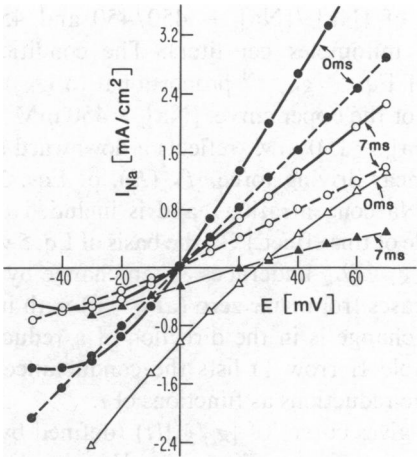

FIGURE 5 Instantaneous current-voltage curves following point *c* (Fig. 1) for $t = 0$ and 7 ms. The four curves crossing the origin (○, ●) were obtained with $[Na]_i = [Na]_e = 450$ mM. Of these the continuous curves are with $[Ca]_e = 100$ mM, and the interrupted (dashed [---]) curves with $[Ca]_e = 4$ mM. Note the partial calcium "block" for negative (inwardly directed) sodium currents in the presence of [Ca] = 100 mM (continuous curves [—] with open [○] and filled [●] circles). Note also the virtual linearity of the curve for $t = 0$ and $[Ca]_e = 4$ mM (dashed curve [---] with filled circles [●]). The remaining two curves (△, ▲, with positive reversal potentials) are for $[Na]_i = 150$ mM, $[Na]_e = 450$ mM, and $[Ca]_e = 4$ mM. Conditioning depolarization was −30 mV for all curves identified as 7 ms.

Conductance Steps Associated with *E* Steps $+70 \rightarrow -30$ mV

Ratios of chord conductance, $[g_c/g_d](t)$, were derived from the unnormalized current ratios, $[I_c/I_d](t)$, by use of the equation

$$[g_c/g_d](t) = \frac{[E^+ - E_{Na}(t)]}{[E^- - E_{Na}(t)]}\,[I_c/I_d](t) \qquad (6)$$

where $E^- = 70$ mV, $E^+ = -30$ mV, and $E_{Na}(t)$ is the measured reversal potential as a function of t. Fig. 6 gives plots of g_c/g_d vs. t for $[Ca]_e = 4$ and for the two sodium

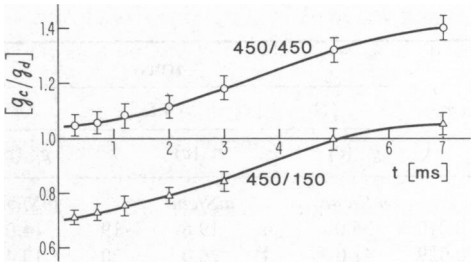

FIGURE 6 Ratios of chord conductances, g_c/g_d (defined by Eq. 6), as functions of t for the two sodium concentration gradients of $[Na]_e/[Na]_i = 450/450$ (○) and 450/150 (△). $[Ca]_e = 4$ mM for both curves. Conditioning depolarization was 0 mV. Membrane potentials at points *c* and *d* were +70 and −30 mV, respectively. Deviations from unity in the upper curve imply a conductance step during the voltage transition $c \rightarrow d$ (see text). The difference in the two curves gives the measure of the sensitivity of the analysis to changes in the factor f_{Na} of Eq. 3.

gradients of $[Na]_e/[Na]_i$ = 450/450 and 450/150 (all values in millimoles per liter). The conditions for the validity of Eq. 5 (g_{Na}^{chord} proportional to Q_{Na}) are nearly satisfied for the upper curve, $[Na]_i$ = 450 mM. (The lower curve, $[Na]_i$ = 150 mM, reflects a downward shift due to the nonlinear driving force, $f_{Na}(E)$, of Eqs. 3 and 4 for unequal Na concentrations, and is included to show the magnitude of this effect.) On the basis of Eq. 5 we conclude that the $\hat{g}_{Na} \cdot Q_{Na}$ undergoes a step change by an amount that increases from near zero (at $t = 0$) with increasing t. The step change is in the direction of a reduced conductance. Table II (row 1) lists the conductances and their percentage reductions as functions of t.

Fig. 7 gives curves of $[g_c/g_d](t)$ (defined by Eq. 6) for four calcium concentrations with $[Na]_i = [Na]_e$ = 450 mM. This family of curves converges rapidly for $[Ca^{++}]_e \leq$ 10 mM. The convergence gives confidence that an extrapolation to zero calcium would lie within the experimental error of the curve for 4 mM calcium, which therefore represents the behavior of conductance in the absence of calcium blockade ($r_{Bl} = 0$).

Table II (rows 2–4) lists calculated percentage changes in $\hat{g}_{Na}Q_{Na}$ for the higher values of $[Ca^{++}_e]$ based on the data presented in Figs. 4 and 7. The calculation of these numbers involves compensation for the fraction of gated open channels that are blocked by calcium. Values of r_{Bl} (−30 mV) were determined on the assumptions that there is no step change in $\hat{g}_{Na}Q_{Na}$ for $t = 0$ and that the degree of the calcium blockade is independent of t, $r_{Bl} = 1 - 1/[g_c/g_d](t = 0)$. From the Table, in conjunction with Eqs. 2, 3, and 5, it appears that the percentage reduction in $\hat{g}_{Na}Q_{Na}$ increases slightly with increasing calcium.

Depolarizing Transitions: −30, +20 → +70 mV

Due to the very rapid change in the state of activation at E = +70 mV it is impossible to reliably extrapolate the current trace across the capacitative transient at point *b* (Fig. 1) for a prepotential of −30 mV. It is therefore impossible to determine the ratio I_a/I_b from those prepulse data.

Data obtained for a prepulse of +20 mV, however, show little additional activation at +70 mV. These data admit a reliable extrapolation of the current at point *b*. The result is negative in the sense that the current ratios, I_a/I_b, remain constant as a function of t when the raw data are compensated for a small shift in E_{Na}. Further, the conductance ratio g_a/g_b remains near unity for $[Na]_i = [Na]_e$ = 450 mM and $[Ca]_e$ = 4 mM.

TABLE II

Ca^{++}	r_{Bl}	t(ms) 1.2		4.5		7.0	
		$g_{Na}(c)$	%	$g_{Na}(c)$	%	$g_{Na}(c)$	%
mM		*mS/cm²*		*mS/cm²*		*mS/cm²*	
4	0.010	35.0	−4	19.6	−19	14.0	−25
10	0.029	41.0	−4	26.0	−20	19.4	−26
40	0.107	51.6	−4	33.2	−21.5	25.4	−28
100	0.296	66.8	−4	46.6	−22.5	36.4	−29

Conductances at +70 mV (Fig. 1, point *c*) and the percentage reductions in $\hat{g}_{Na}Q_{Na}$ (see Methods, Eqs. 3 and 5, and text) following the potential step to −30 mV (Fig. 1, point *d*) for three values of t and four external calcium concentrations. Conditioning depolarization was −30 mV. $[Na]_i = [Na]_e$ = 450 mM. Values for the blocking parameter at −30 mV, r_{Bl}, due to calcium were computed from the data given in Fig. 7 for $[Na]_i = [Na]_e$ = 450 mM (see text).

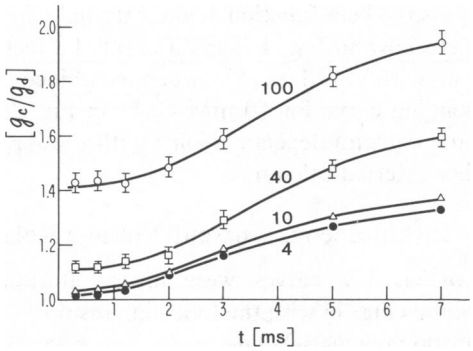

FIGURE 7 Ratios of chord conductances, g_c/g_d (Eq. 6), as functions of t for calcium concentrations of 100 (○), 40 (□), 10 (△), and 4 mM (●). Sodium concentrations were 450 mM on both membrane sides. Conditioning depolarization was 0 mV. Membrane potentials at points *c* and *d* were +70 and −30 mV, respectively. The systematic elevating of the curves with increasing $[Ca]_e$ is mainly due to a reduced conductance, g_d, resulting from channel blockade by calcium ions.

Repolarizing Transitions

Conductance steps derived from current records across potential steps from +70 mV to values ≥0 mV are zero to within experimental error. Current variations following the initial 15 μs at point *d* are small, giving a high degree of reliability in the measurements. It is interesting to note that these voltage steps are entirely outside of the gating range of the Hodgkin-Huxley model in the sense that the steady state values of both activation ($m_\infty \sim 1.0$) and inactivation ($h_\infty \sim 0$) are virtually voltage-independent in the region of 0 to +70 mV.

In contrast to these negative results, repolarizing transitions to −70 mV appear to involve sizeable conductance steps. All steps are in the direction of reduced conductances. Percentage reductions in $\hat{g}_{Na}Q_{Na}$ (Methods, Eqs. 3 and 5) for voltage steps from *e* to *f* (Fig. 1) are given in Table III.

DISCUSSION

A reduction in the sodium conductance following a voltage perturbation has been previously described by Schauf and Baumann (1981) in *Myxicola* giant axons. In those experiments the perturbation consisted of large (+200 mV) depolarizing pulses (on the order of 100 μs duration)

TABLE III

E^-	t(ms)			
	1.2	3	5	7
	%	%	%	%
+40	−4	−16	−26	−29
0	−4	−15	−25	−28
−30	−4	−9	−14	−17

Percentage reductions in $\hat{g}_{Na}Q_{Na}$ following the voltage step from E^-(mV) to −70 mV as functions of t. Conditioning depolarization was +20 mV. Data are for axons bathed in $[Na]_i = [Na]_e = 450$ mM and $[Ca]_e = 10$ mM.

introduced on an otherwise single level voltage-clamp depolarization to −30 mV. From those current records it appears that the magnitudes of the current traces of the perturbed pulses remain a fixed fraction (<1) of the unperturbed magnitudes throughout the latter portion of the trace. Here we have shown that the conductance appears to change on a time-scale of ≤ 10 μs in response to a certain class of voltage steps in squid axons. The conductance step response depends on the history of depolarization as shown by its dependence on the variable t (defined in Fig. 1). The speed limitation of the clamp leaves the actual course of the conductance transition temporally unresolved. Nevertheless the conductance shift is at least, and possibly much greater than, approximately two orders of magnitude faster than the Hodgkin Huxley model $\tau_m(-30\text{ mV}) \cong 0.5$ ms at 5°C. The conductance changes at −30 mV after the step change do subsequently relax with a time constant of ~0.5 ms.

The fast (microseconds) conductance shifts appear to occur only when at least a portion of the potential range traversed in the voltage step is in the gating range. "Gating range" is defined here as those membrane potentials, E, for which $dm_\alpha/dE \neq 0$, approximately −70 to +20 mV. Among the possible mechanisms that might be responsible for the phenomenon are variations on the theme of multiple populations of sodium channels, each with multiple conductance states, and each in turn conducting with different instantaneous I-V characteristics. An appealing model consists of two populations with different gating time constants and different instantaneous I-V curves. The step change in "conductance" is then explained on the basis of each population stepping along its own I-V curve during a voltage step. The dependence on time of conditioning depolarization is explained by the different rate constants for the gating of the two populations.

Another possible mechanism, unrelated to gating, is an "anomalous" rectification of the channels. An otherwise gated open channel may become an outwardly directed rectifier (the type required to explain the present results) even with symmetrical concentrations of the conducting ions if between sites (energy minima) along the channel the activation energy increases near the external surface or decreases near the internal surface end of the channel. If these changes in activation energy are voltage and time dependent they could explain the results. Such changes can affect the instantaneous I-V properties of the channel, but not its reversal potential (Woodbury, 1971). On the other hand, mechanisms or charge movements that increase or reduce the concentration of conducting ions near the pores, beyond those due to unstirred layer effects, appears to be ruled out on the basis of the behavior of the reversal potentials of the instantaneous I-V curves.

Without diminishing the viability of certain of the above possibilities which cannot be further evaluated on the basis of the present data alone, we proceed to analyze the implication of the results assuming a single population of sodium channels and that we are dealing with a gating phenomenon. The simplest kinetic model (although by no means the only model) for sodium activation is the linear scheme

$$C_1 \underset{k'_1}{\overset{k_1}{\rightleftharpoons}} \cdots \underset{k'_{l-2}}{\overset{k_{l-2}}{\rightleftharpoons}} C_{l-1} \underset{k'_{l-1}}{\overset{k_{l-1}}{\rightleftharpoons}} C_l \underset{k'_l}{\overset{k_l}{\rightleftharpoons}} 0 \qquad (7)$$

where C represents closed channel conformations and 0 an open one. For the Hodgkin-Huxley model $l = 3$, $k_j = (4 - j)\alpha_m(E)$ and $k'_j = j\beta_m(E)$ (cf., Armstrong and Matteson, 1983). In its simplest form this model assumes no delayed local potential adjustments within the membrane so that the rate constants are a direct function of the transmembrane field only.

The data presented herein are most easily explained if this assumption is removed, and the rate constants themselves are given a time dependence. Physically, this is equivalent to certain delayed adjustments in the local potential energy within the membrane (Fig. 8). The linear scheme (Eq. 7) is illustrative and the arguments to follow apply equally well to kinetics containing cyclical components in which the open state is directly connected to more than one closed state. Further, the conformational changes may involve transitions within a molecule or they may involve subunit assembly or disassembly (cf. Baumann and Easton, 1981). We assume only that the principle of

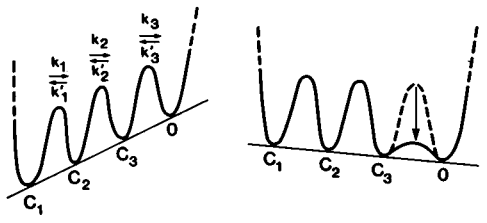

FIGURE 8 Hypothetical potential energy profiles associated with the conformational changes of activation gating at two membrane potentials: *Left E* near the resting potential or slightly hyperpolarized. *Right E* at a moderately depolarized value (0 to +20 mV). The rate constants k_j and k'_j may be formally related to the Hodgkin-Huxley model α_m and β_m (see text). The decreased barrier between C_3 and 0 is due to a hypothetical molecular process represented by Eq. 9.

detailed balance is obeyed and, for simplicity, that there is a single open configuration.

Fig. 8 shows hypothetical potential energy profiles representing barriers to molecular rearrangements associated with the activation gating process of Eq. 7 for two membrane potentials, at least one of which is in the gating range. If, upon depolarization, the final barrier between C_3 and 0 relaxes to a smaller height on an independent time scale, the steady state probability distribution among the states C_j and 0 will remain unchanged for a given voltage (i.e., $m_x(E)$ remains unchanged). This follows because the activation energy contained in both the forward and backward rate constants across a given barrier changes by the same amount, $\delta G^{\ddagger}$, leaving the zero probability flux of the steady-state distribution,

$$P_j k_j - P_{j+1} k'_j = 0 = P_j k_j e^{-\delta G^{\ddagger}/RT} - P_{j+1} k'_j e^{-\delta G^{\ddagger}/RT}, \quad (8)$$

unchanged in the absence of an external field change. Because $\delta G^{\ddagger}$ enters exponentially, a two orders of magnitude increase in the rate constants is equivalent to a barrier reduction by a factor of 4.6. With a lower barrier, a voltage step will cause a more rapid redistribution between states C_3 and 0, resulting in the rapid conductance shifts. Such a shift will occur only if the voltage step overlaps at least partially the gating range, because only in that range is the overall profile of the potential barriers (Fig. 8) responsive to a voltage change.

The barrier reduction would be the result of an additional but concurrent molecular process that, in simplest terms, is given by

$$A_1 \rightleftharpoons \cdots \rightleftharpoons A_{n-1} \rightleftharpoons A_n \quad (9)$$

where A_j represents conformational states corresponding to different barrier heights between C_3 and 0 in Fig. 8. The sigmoidal nature of the curves in Figs. 3, 4, 6, and 7 implies that at least three states A are involved. Values of at least some of the rate constants of this process must clearly be voltage dependent, and on the basis of the data presented herein, they must be in the range of 0.1 to 1.0 ms^{-1}. In this model, then, "gating currents" are due (at least in part) to molecular rearrangements associated with the change in barrier height. Such a parallel process will have its own voltage range of variation that may partly overlap, but generally not coincide with the gating range as defined above. This, and possibly similar processes affecting the rate constants among closed channel conformations may be responsible for the gating currents at hyperpolarized potentials (for example, see Bezanilla and Taylor, 1978) in a region where little or no sodium conductance change is observed.

The conformation change associated with the conductance step would also contribute to the gating current; because it is a voltage-dependent step it cannot be an electrically silent step. These gating currents are likely to be among the earliest components of the current records whose rising phase too is so rapid that it may be temporally unresolved (cf. French and Horn, 1983, p. 328).

Molecular processes of the type represented by Eq. 9 may be operative in at least two other phenomena: (*a*) The so-called Cole-Moore effect (Cole and Moore, 1960) may involve a molecular rearrangement that increases the height of the barrier between C_1 and C_2 of a scheme similar to Eq. 7 and applied to potassium-channel as well as sodium-channel gating (e.g., Keynes and Rojas, 1976) with hyperpolarizing prepotentials. Transitions $C_1 \rightleftharpoons C_2$ are then markedly slowed upon depolarization until the barrier is again reduced with some delay following depolarization. The voltage-dependent kinetics of this hypothetical process are primarily restricted to the hyperpolarized region and may contribute to the gating currents at hyperpolarized potentials. (*b*) Current records of single channels often show brief interruptions of the open state. This "bursting" appears to be more pronounced in the K-channel records of Conti and Neher (1980) than in the Na-channel records of Sigworth and Neher (1980). The source of this bursting may, of course, lie in random constrictions of the ion channel that has no connection with voltage gating. However, if voltage gating is involved, then at least some of the rate constants connecting the open with its nearest closed state conformations must be relatively large (cf. Conti and Neher, Eq. 2). If one assumes that the potential barrier connecting these two states is reduced only after a delay of some milliseconds following depolarization, one might expect the bursting phenomenon under steady-state conditions such a those of the K-channel recordings. Bursting would be somewhat suppressed in the Na-channel records because the channel would be substantially inactivated before its onset.

REFERENCES

Adelman, W. J., Jr., J. Moses, and R. V. Rice. 1977. An anatomical basis for the resistance and capacitance in series with the excitable membrane of the squid giant axon. *J. Neurocytol.* 6:621–646.

Adelman, W. J., Jr., and R. J. French. 1978. Blocking of the squid axon potassium channel by external caesium ions. *J. Physiol. (Lond.)*. 276:13–25.

Armstrong, C. M., and D. R. Matteson. 1983. Activation gating of nerve sodium channels: simulations. *Biophys. J.* 41(2, Pt. 2):223 *a*. (Abstr.)

Baumann, G., and G. S. Easton. 1981. Markov process characterization of a single channel gating site. *J. Theor. Biol.* 93:785–804.

Bezanilla, F., and R. E. Taylor. 1978. Temperature effects on gating currents in the squid giant axon. *Biophys. J.* 23:479–484.

Binstock, L., W. J. Adelman, Jr., J. P. Senft, and H. Lecar. 1975. Determination of the resistance in series with the membranes of giant axons. *J. Membr. Biol.* 21:25–47.

Chiu, S. Y. 1976. Observations of sodium channel inactivation in frog nerve. *Biophys. J.* 16(2, Pt. 2):25 *a*. (Abstr.)

Cole, K. S., and J. W. Moore. 1960. Potassium ion current in the squid giant axon: dynamic characteristic. *Biophys. J.* 1:1–14.

Cole, K. S., and U. Kishimoto. 1962. Platinized silver chloride electrode. *Science (Wash., DC)*. 136:381–382.

Cole, K. S. 1968. Membranes, Ions and Impulses. University of California Press, Berkeley. 1–569.

Conti, F., and E. Neher. 1980. Single channel recordings of K^+ currents in squid axons. *Nature* (*Lond.*). 285:140–143.

Fishman, H. M. 1973. Low impedance capillary-electrode for wideband recording of membrane potential in large axons. *IEEE* (*Inst. Electr. Electron. Eng.*) *Trans. Biomed. Eng.* 20:380–382.

Fohlmeister, J. F., and W. J. Adelman. 1982 *a*. Periaxonal surface calcium binding and distribution of charge on the faces of squid axon potassium channel molecules. *J. Membr. Biol.* 70:115–123.

Fohlmeister, J. F., and W. J. Adelman. 1982 *b*. Anomalous potassium channel gating rates as functions of calcium and potassium ion concentrations. *Biophys. J.* 37:427–431.

French, R. J., and R. Horn. 1983. Sodium channel gating: models, mimics and modifiers. *Annu. Rev. Biophys. Bioeng.* 12:319–356.

Hodgkin, A. L., and A. F. Huxley. 1952. A quantitative description of membrane current and its application to conduction and excitation in nerve. *J. Physiol.* (*Lond.*). 117:500–544.

Keynes, R. D., and E. Rojas. 1976. The temporal and steady-state relationships between activation of the sodium conductance and movement of the gating particles in the squid giant axon. *J. Physiol.* (*Lond.*). 255:157–189.

Schauf, C. L. 1974. Sodium currents in *Myxicola* axons. Nonexponential recovery from the inactive state. *Biophys. J.* 14:151–158.

Schauf, C. L., and G. Baumann. 1981. Experimental evidence consistent with aggregation kinetics in the sodium current of *Myxicola* giant axons. *Biophys. J.* 35:707–714.

Sigworth, F. J., and E. Neher. 1980. Single sodium channel currents observed in cultured rat muscle cells. *Nature* (*Lond.*). 287:447–449.

Taylor, R. E., C. M. Armstrong, and F. Bezanilla. 1976. Block of sodium channels by external calcium ions. *Biophys. J.* 16(2, Pt. 2):27 *a*. (Abstr.)

Woodbury, J. W. 1971. Eyring rate theory model of the current voltage relationships of ion channels in excitable membranes. *In* Chemical Dynamics. Papers in Honor of Henry Eyring. J. O. Hirschfelder and D. Henderson, editors. John Wiley & Sons, Inc., New York. 601–617.